

The significance of rate effects in modelling the Sackville test embankment

R. Kerry Rowe and Sean D. Hinchberger

Abstract: It has been reported that conventional methods of analysis could not adequately describe all aspects of the behaviour of a geotextile-reinforced test embankment constructed to failure on a soft clayey silt with some organics at Sackville, New Brunswick (Canada). This paper presents the results of an analysis of the Sackville embankment using a fully coupled elasto-viscoplastic constitutive model with an elliptical cap yield surface. The importance of modelling the rate sensitive characteristics of the Sackville foundation soil is demonstrated. A comparison of calculated and measured behaviour of the Sackville test embankment demonstrates that the single elasto-viscoplastic yield surface model adequately described much of the measured time-dependent behaviour of the Sackville test embankment including post construction increases in pore pressure, deformation and reinforcement strain.

Key words: Embankment; soft soil; geosynthetic; reinforcement; analysis; field case, viscoplasticity

Resumé : L'on a fait état du fait que les méthodes conventionnelles d'analyse ne pouvaient pas décrire adéquatement tous les aspects du comportement d'un remblai d'essai armé de géotextile construit jusqu'à la rupture sur un silt argileux mou contenant des matières organiques à Sackville, Nouveau Brunswick (Canada). Cet article présente les résultats d'une analyse du remblai de Sackville au moyen d'un modèle de comportement élasto-viscoplastique complètement couplé avec une surface d'état limite elliptique. L'on démontre l'importance de la modélisation des caractéristiques de sensibilité à la vitesse de déformation du sol de fondation de Sackville. Une comparaison des comportements calculé et mesuré du remblai d'essai de Sackville démontre que le simple modèle élasto-viscoplastique de surface d'état limite décrit adéquatement une bonne part du comportement fonction du temps mesuré dans le cas du remblai d'essai de Sackville, incluant l'augmentation après construction de la pression interstitielle, de la déformation et de l'étirement de l'armature.

Mots clés : remblai, sol mou, géosynthétique, armature, analyse, cas de terrain, visco-plasticité.

[Traduit par la Rédaction]

Introduction

The Sackville test embankment (Rowe et al. 1995; see also Fig. 1) was constructed with two objectives in mind. The first was to provide data that could be used in assessing the ability of conventional methods of analysis for predicting the behaviour of a geotextile-reinforced embankment on an organic clayey silt foundation. The second was to provide data that could be used to develop improved methods of analysis if existing methods proved inadequate. To address the first objective, Rowe et al. (1996) analyzed the embankment behaviour using a fully coupled large-strain elasto-plastic analysis and a modified Cam-clay model for the organic clayey silt. The analysis captured many features of the embankment behaviour; however, it was concluded that even allowing for consolidation, the elasto-plastic formulation was not adequate for accurately and simultaneously predicting multiple characteristics of the embankment behaviour (e.g., vertical and horizontal defor-

mations, pore pressure, and geotextile strains). They also concluded that the discrepancy was likely due to the rate sensitive nature of the soil and the consequent "progressive failure" of the foundation soil.

This paper addresses the second objective; namely, developing an alternative analysis and testing it against the observed behaviour of the Sackville embankment. The analysis is based on the use of an elasto-viscoplastic elliptical cap model to describe the rate sensitive characteristics of the Sackville foundation soil. Details of the constitutive model will be described and the results from the finite element analysis will be compared with the observed embankment behaviour. Particular attention will be paid to the ability of the model to describe the time-dependent deformations and excess pore pressures.

Theoretical treatment of rate effects

The rate sensitive characteristics of the Sackville foundation soil were modelled using Perzyna's (1963) theory of overstress-viscoplasticity and an elliptical yield function of the form proposed by Chen (1982). Figure 2 shows the geometry of an elliptical yield surface where $\sigma'_m = (\sigma'_1 + \sigma'_2 + \sigma'_3)/3$ is the mean effective stress; $\sigma_{my}^{(s)}$ is the current yield surface intercept with the σ'_m axis; R_c is the yield surface aspect ratio in $(2J_2)^{1/2} - \sigma'_m$ stress space, J_2 is the sec-

Received December 18, 1996. Accepted March 5, 1998.

R.K. Rowe. Department of Civil and Environmental Engineering, University of Western Ontario, London, ON N6A 5B9, Canada. e-mail. r.k.rowe@uwo.ca.

S.D. Hinchberger. Trow Consulting Engineers Ltd., 1595 Clark Boulevard, Brampton, ON L6T 4V1, Canada.

Fig. 1. Cross section of Sackville test embankment and location of instrumentation (from Rowe et al. 1995).

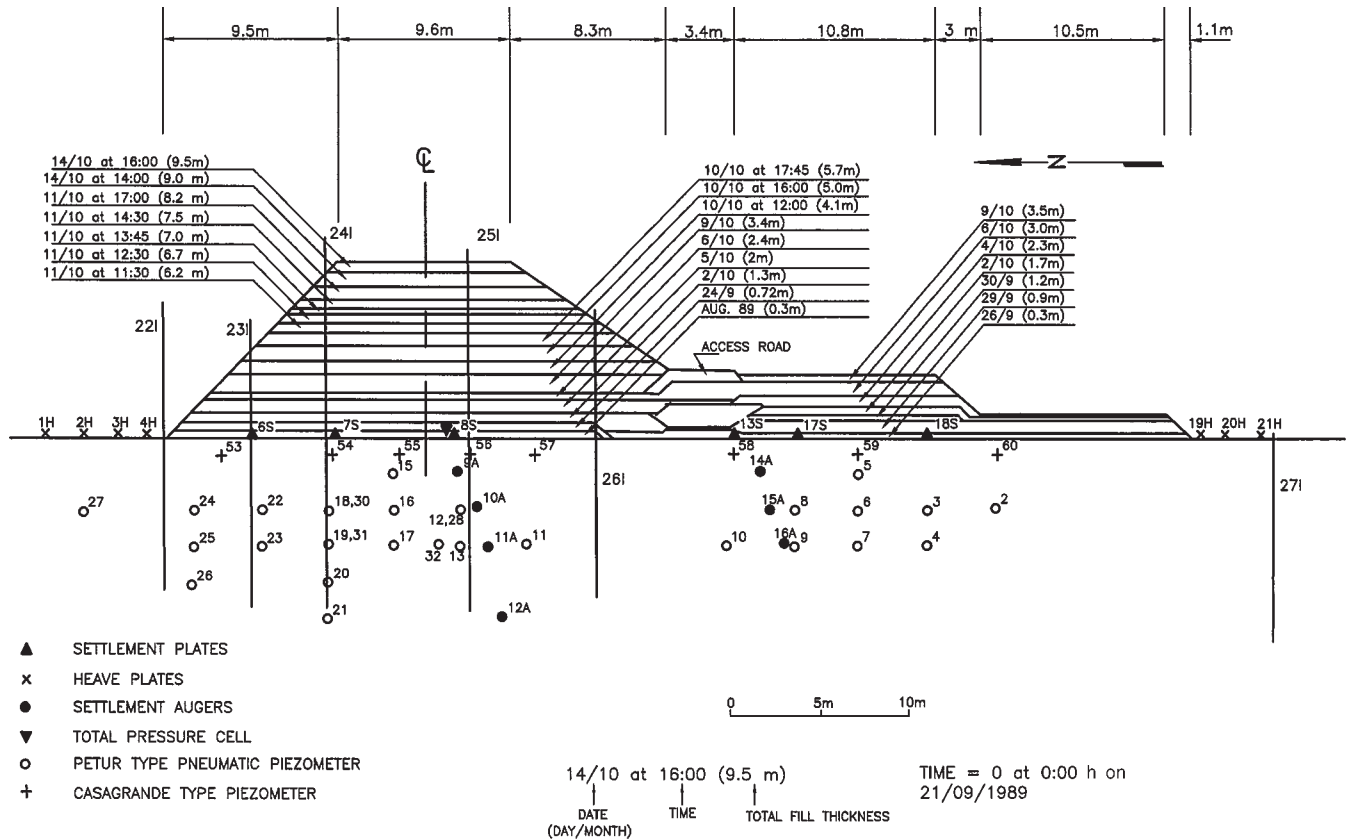
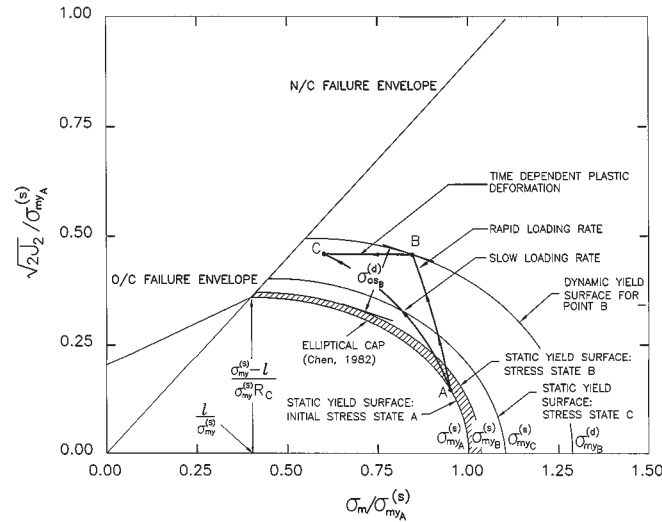


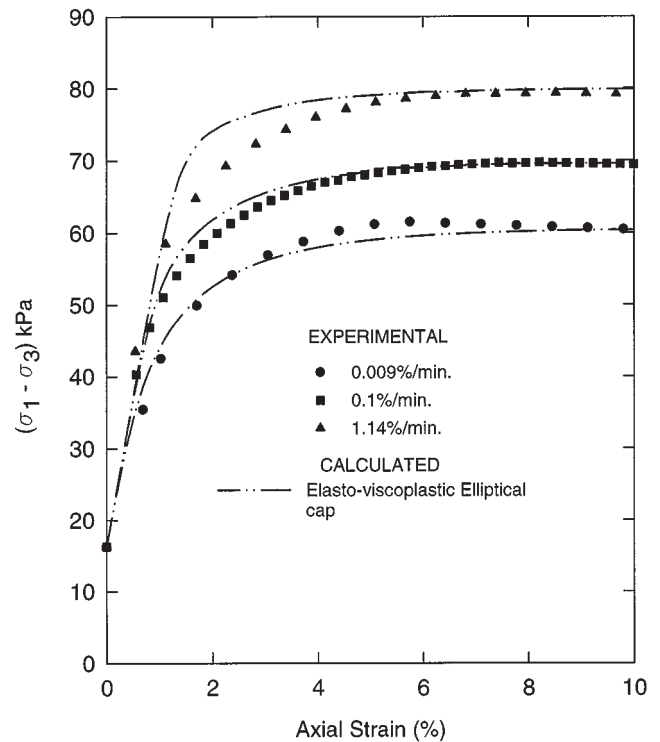
Fig. 2. Dynamic stress path, overstress measurement and geometry of elliptical yield surface (modified from Chen 1982).



ond invariant of the deviatoric stress tensor; and ℓ is the mean effective stress corresponding to the centre of the ellipse. Failure is defined using a Drucker-Prager failure envelope with a slope M and M^* in the normally and overconsolidated range, respectively. The mathematical details defining this model are given in Appendix A.

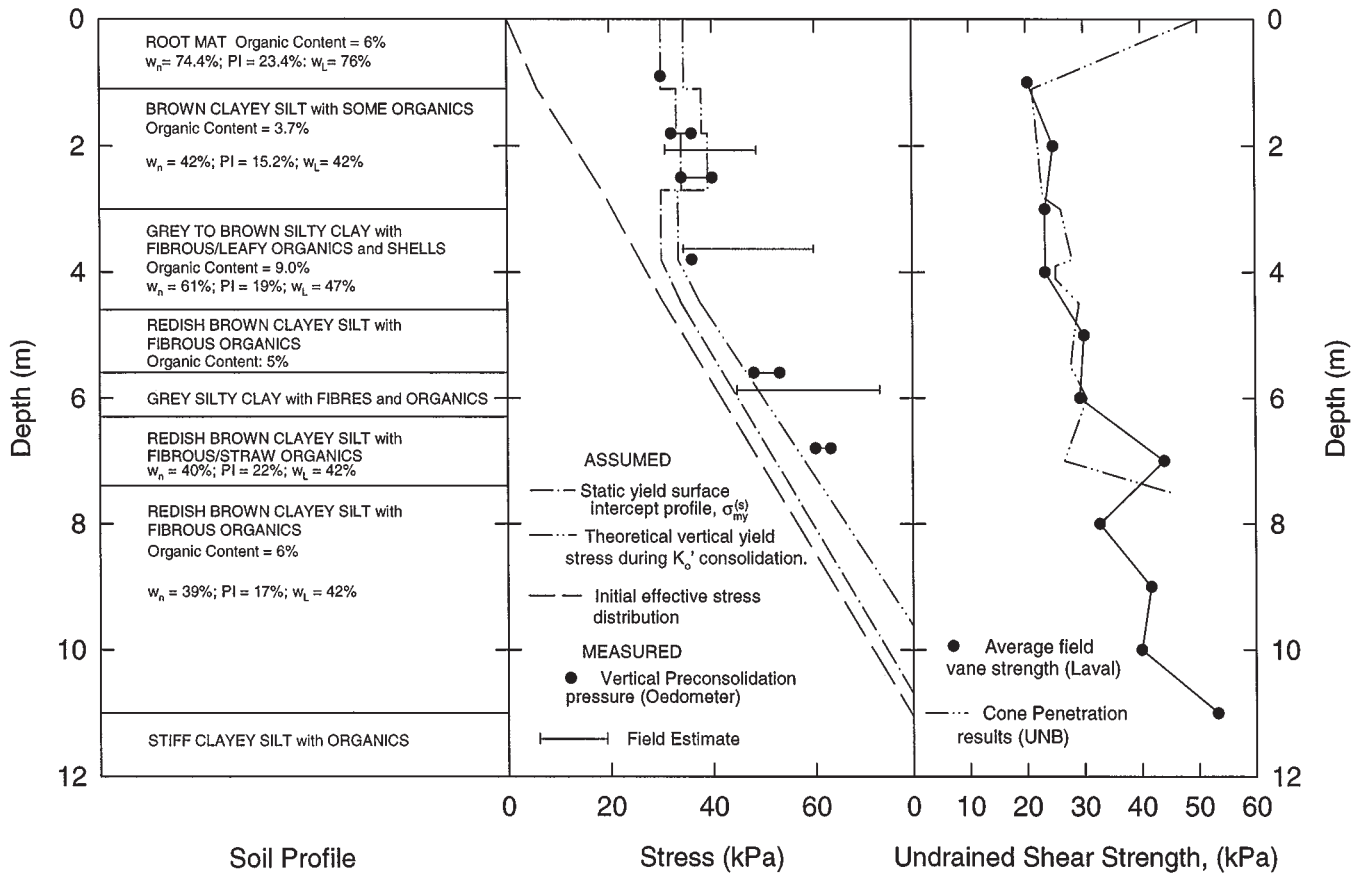
To conceptually illustrate the characteristics of the model, consider a point in the soil that is initially normally consolidated under K'_0 stress (point A in Fig. 2). The application of an embankment load may cause the stress state at that point

Fig. 3. Calculated and measured deviator stress versus axial strain response during CAU triaxial shear (3.65–3.85 m).



to exceed yield and move along the dynamic stress path A–B shown in Fig. 2. Negative elastic volumetric strain

Fig. 4. Summary of subsurface profile at the site of the Sackville test embankment (modified from Rowe et al. 1995).



(elastic unloading) occurs for stress path A–B. For undrained conditions, positive plastic volumetric strains of equal magnitude to the negative elastic volumetric strains occur to maintain conditions of constant volume deformation. The plastic volumetric strains that occur for stress path A–B cause the static yield surface to expand in stress space to $\sigma_{myB}^{(s)}$.

At stress state B, the soil is overstressed by an amount $\sigma_{os}^{(d)}$ as shown in Fig. 2. During constant embankment loads, time-dependent plastic deformations proportional to the amount of overstress, $\sigma_{os}^{(d)}$, are predicted by the model and the dynamic stress state will move with time under undrained conditions similar to stress path B–C. During this process, additional time-dependent excess pore pressures and plastic strains are generated and the plastic volumetric strains cause the static yield surface to expand from $\sigma_{myB}^{(s)}$ to $\sigma_{myC}^{(s)}$. It is important to note that, for undrained conditions, negative elastic volumetric strains (elastic unloading) of equal magnitude to the plastic volumetric strains will occur for stress path B–C, thus maintaining conditions of constant volume. Given sufficient time, the dynamic stress state will approach the static yield surface and the full plastic strains associated with conventional plasticity will have accumulated. It should also be noted that stress path A–C is also possible during embankment construction provided that the loading rate is sufficiently low. The theoretical response of elasto-viscoplastic soil models during undrained loading conditions have also been described qualitatively by Adachi and Oka (1982) and Katona and Mulert (1984).

In addition to the foregoing qualitative description, Fig. 3 shows the comparison of calculated (theoretical) and measured axial load versus axial strain for Sackville soil from a depth of 3.65–3.85 m. The measured undrained shear strength of the Sackville soil was found to be rate dependent during Consolidated Anisotropic Undrained (CAU) triaxial tests. The theoretical elasto-viscoplastic yield surface model (described qualitatively above and in detail in Appendix A) can model the strain rate dependency measured during undrained shear as indicated by the good agreement with the measured behaviour in Fig. 3. Similar results were obtained for Sackville soil from depths of 2.3–2.5, 5.5–5.7, and 6.65–6.86 m (Hinchberger 1996).

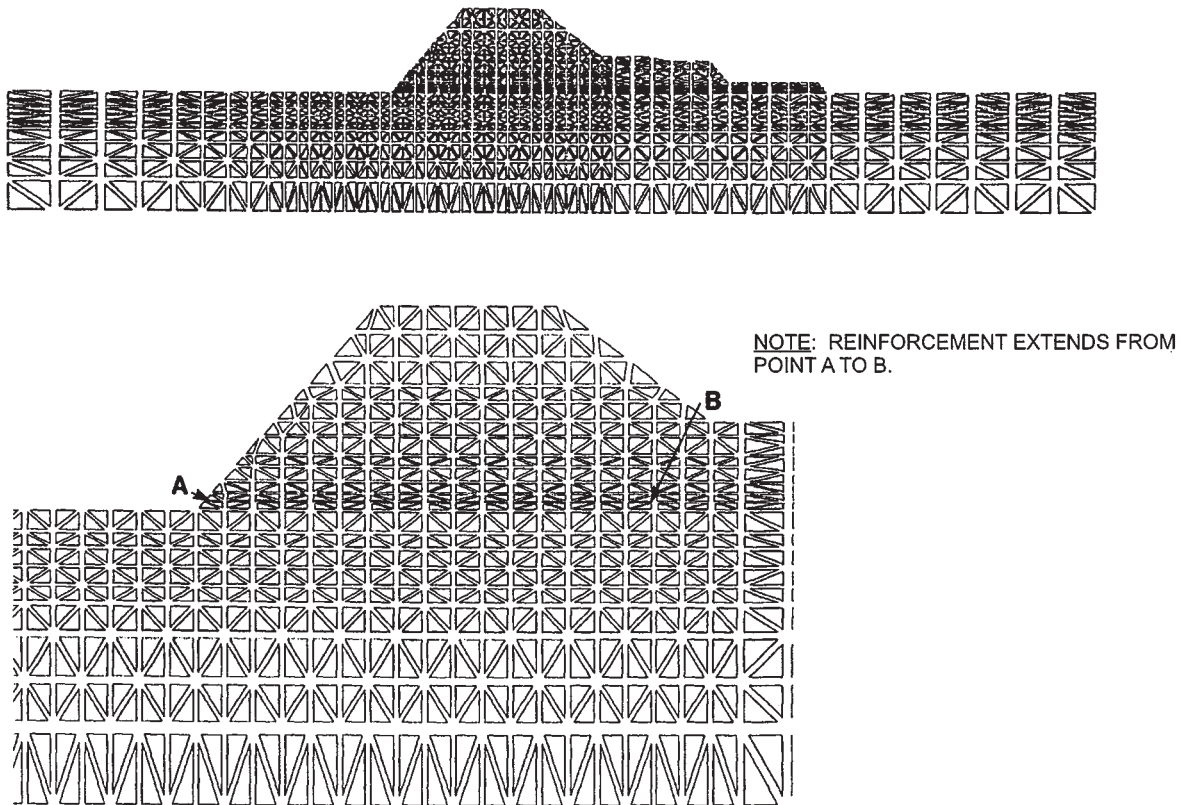
It is significant that the model implies that

- the shear strength during undrained shear is strain rate dependent;
- for a given final load the shear strength can exceed the long term or static shear strength and, hence, the soil will deform at a rate that is proportional to the amount of overstress, $\sigma_{os}^{(d)}$; and
- loads in excess of yield are permissible.

Under these circumstances, plastic flow will occur in a time-dependent manner and the stress state will tend toward the yield and failure surface along a stress path similar to BC in Fig. 2.

The elliptical cap elasto-viscoplastic constitutive model with the Drucker–Prager failure envelope was coupled with Biot consolidation theory and incorporated into the finite element program AFENA originally developed by Carter and

Fig. 5. Finite element mesh used to obtain the calculated behaviour of the Sackville test embankment.



Balaam (1990) and subsequently modified by the authors. The finite element implementation of the elasto-viscoplastic elliptical cap model used in this paper and its application for modelling the rate sensitive characteristics of the Sackville foundation soil are described by Hinchberger (1996).

Finite element analysis

Figure 1 shows the cross section of the reinforced section of the Sackville test embankment that is modelled in this paper, together with the construction sequencing and the location of instrumentation used to monitor displacements and excess pore pressures. A summary of the geotechnical profile is shown in Fig. 4. The subsurface profile has been described in detail by Rowe et al. (1995; 1996) and Rowe and Hinchberger (1995).

For the present analyses, the foundation and the embankment were discretized using 1568 six-noded linear strain triangular elements. The foundation soil was assumed to have an impermeable rough rigid boundary at a depth of 14 m. The foundation layer was modelled to a distance of 50 m beyond the embankment toe and 30 m beyond the toe of the south berm. At the lateral boundaries, a smooth permeable boundary condition was assumed. Six-noded slip elements were used to model the interface between the embankment fill and foundation soil and the interface between the reinforcement and embankment fill. The geosynthetic reinforcement was discretized using two-noded bar elements. The finite element mesh (see Fig. 5) included three degrees of freedom per node for foundation soil elements to account for displacements and pore pressures.

For the analysis presented in this paper, small strain theory was used. Carter et al. (1979) showed that for a rigid footing with displacements less than 25% of the thickness of the foundation layer, the difference between displacements calculated using finite deformation theory and small strain theory was minimal. Based on the findings of Carter et al. (1979), the fact that the vertical settlements at Sackville were less than 20% of the foundation layer thickness, and the previous experience of Rowe et al. (1996) who did use large deformation theory to analyze the Sackville embankment, it was considered reasonable to use small strain theory for the present analysis.

Selection of parameters

Profile of preconsolidation pressures

The initial groundwater conditions were essentially hydrostatic and the groundwater table was at the ground surface. Morin et al. (1983) and Leroueil et al. (1983) demonstrated that the excess pore pressures generated beneath embankments constructed quickly on a clayey foundation can be used to estimate the in situ or field preconsolidation pressure. To obtain the range of field preconsolidation pressures for the Sackville foundation soil, an elastic finite element analysis was used to calculate the change in vertical stress, $\Delta\sigma_v$, at piezometers 15, 16, and 17 (see Fig. 1) during construction of the Sackville test embankment. The changes in vertical stress were then plotted versus the measured change in excess pore pressures, Δu . Yielding was considered to have occurred at a fill thickness where the incremental

Table 1. Parameters controlling the vertical permeability of the soil (see eq. [2]).

epth (m)	e_r	C_k	k_r (m/s)
0.0–1.1	2.4	0.22	1.7×10^{-8}
1.1–1.8	2.4	0.22	1.7×10^{-8}
1.8–2.7	1.2	0.16	8.3×10^{-9}
2.7–4.4	2.4	0.22	1.7×10^{-8}
4.4–5.8	2.4	0.22	1.7×10^{-8}
5.8–10.0	1.2	0.16	8.3×10^{-9}
10.0–14.0	1.2	0.16	8.3×10^{-9}

change in excess pore pressure was approximately equal to the incremental increase in vertical stress, e.g., $\Delta\sigma_v = \Delta u$.

Figure 4 shows the range of field preconsolidation pressures inferred from the excess pore pressures measured at piezometers 15, 16, and 17, and the preconsolidation pressures measured during standard incremental oedometer and triaxial consolidation tests. The preconsolidation pressures measured during conventional laboratory consolidation tests are in agreement with the range of inferred field preconsolidation pressures at depths of 2 and 6 m. Piezometer 16, at 4 m depth, is suspected of having had a leaking seal and hence the inferred field preconsolidation pressure from this piezometer appears to be too high.

Based on the measured K'_o value of about 0.8 reported by Rowe et al. (1995), the position of the yield surface ($\sigma_{my}^{(s)}$; Fig. 2) was established such that during consolidation, theoretical yielding occurred at a vertical stress approximately corresponding to the measured vertical preconsolidation pressure. For example, for $K'_o = 0.8$, $c'_k = 0.9$ kPa, $M^* = 0.96$, and $R'_c = 1.25$, the relationship between the static yield surface intercept and the vertical preconsolidation pressure is

$$[1] \quad \sigma'_p = 1.11\sigma_{my}^{(s)}$$

where eq. [1] can be derived from the yield surface equation for the elliptical cap model (see Hinchberger 1996). Thus, the yield surface intercept profile used in the analysis (see Fig. 4) has the same shape as the laboratory preconsolidation pressure profile but is approximately 10–15% below the laboratory values.

Foundation properties

The Sackville foundation soil did not exhibit significant anisotropic behaviour during undrained triaxial testing (see Gnanendran 1993) providing some justification for the use of an isotropic elasto-viscoplastic constitutive model based on the elliptical cap yield surface.

Owing to the variable nature of the Sackville foundation soil, the foundation was subdivided into seven subsurface units based on the vane shear strength profile and the geotechnical profile shown in Fig. 4 (to be discussed later). Based on the studies by Gnanendran (1993), the ratio of the horizontal to vertical permeability (hydraulic conductivity), k_h/k_v , was taken to be 4 for soil below a depth of 1.1 m and 10 for the upper 1.1 m (root mat) of the foundation soil.

The vertical permeabilities estimated from the results of triaxial and oedometer consolidation tests were found to de-

crease with decreasing void ratio according to the relationship:

$$[2] \quad k_v = k_r \exp\left[\frac{(e - e_r)}{C_k}\right]$$

where k_r is the reference vertical permeability at the reference void ratio, e_r ; and C_k is the slope of the best fit to the $e - \log(k)$ plot given in Table 1 for each layer.

Table 2 contains a summary of the foundation properties used in the analysis. The viscosity constants and failure envelope for the Sackville soils were estimated from a combination of: (i) constant rate of strain CAU triaxial tests and (ii) CAU triaxial creep tests. Details regarding the estimation of the rate constants (γ^{np} and n) based on these data are given by Hinchberger (1996). Both the compression index, λ , and recompression index, κ , were estimated from standard triaxial and oedometer consolidation tests on samples from depths of 0.9, 1.9, 2.5, 3.8, 5.6, and 6.8 m. A related laboratory investigation verified that the expression proposed by Terzaghi and Peck (1948)

$$[3] \quad \lambda = \frac{C_c}{2.3} = \frac{0.009(w_L - 10)}{2.3}$$

is valid for the Sackville foundation soil. To account for the variability of the compression index for the Sackville foundation soil, the average liquid limit, w_L , for each subsurface unit was used with eq. [3] to select a representative compression index, λ . The recompression index, κ , was estimated based on the ratio of the compression, λ , and recompression, κ , indexes established from the laboratory consolidation tests (Hinchberger 1996). The aspect ratio of the yield surface, R_c , for the Sackville foundation soil was found to range from 1.1 at depths of 5.5–5.8 m to 1.25 at depths of 2.35–2.6 and 3.6–3.85 m. Analyses were performed using a single aspect ratio $R_c = 1.25$ and shear strength parameters $c'_k = 8.0$ kPa, $c' = 6.5$ kPa, and $M = 0.96 \equiv \phi'_{N/C} = 28^\circ$ based on the test results obtained by Gnanendran (1993).

Embankment fill and reinforcement properties

The embankment fill material was modelled as an elastoplastic (inviscous) material with a Mohr–Coulomb failure criterion and a nonassociated flow rule proposed by Davis (1968). The Young's modulus was assumed to be dependent on the minor principle stress and described using Janbu's equation (Janbu 1963) viz.

$$[4] \quad \frac{E'}{P_a} = K_E \left[\frac{\sigma'_3}{P_a} \right]^m$$

where E' is Young's modulus, P_a is the atmospheric pressure, is the minor principal stress, and the values of K_E and m are as given in Table 3. The high strength multifilament woven polyester geotextile reinforcement had a bilinear stress–strain curve that was approximated by two different stiffnesses, J , over the strain ranges 0–1% and 1–13%. The failure strain was 13%. The test procedures used to measure the geotextile reinforcement and embankment fill properties are described by Rowe and Gnanendran (1994).

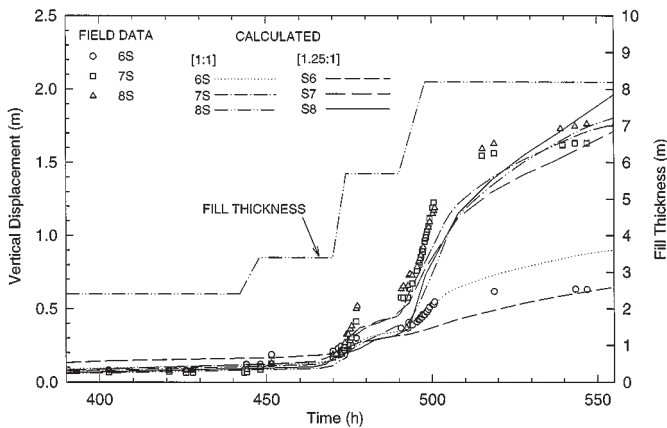
Table 2. Assumed material properties for the analysis of the Sackville test embankment.

Depth (m)	M^*/M	c'_k/c' (kPa)/(kPa)	γ (kN/m ³)	K'_o	e_o	κ	λ	$\dot{\gamma}^{pP}$ ($\times 10^9 \text{ s}^{-1}$)	n
0.0–1.1	0.75/0.96	8.0/6.5	17.8	0.68	2.2	0.055	0.28	5.6	20.0
1.1–1.8	0.75/0.96	8.0/6.5	17.8	0.70	1.2	0.03	0.14	5.0	20.0
1.8–2.7	0.75/0.96	8.0/6.5	17.5	0.70	1.6	0.03	0.22	5.0	20.0
2.7–4.4	0.75/0.96	8.0/6.5	16.5	0.75	1.6	0.05	0.15	5.6	20.0
4.4–5.8	0.75/0.96	8.0/6.5	17.2	0.80	1.5	0.03	0.15	6.1	20.0
5.8–10.0	0.75/0.96	8.0/6.5	17.2	0.80	1.2	0.03	0.15	5.0	20.0
10.0–14.0	0.75/0.96	8.0/6.5	17.2	0.80	1.2	0.03	0.15	5.0	20.0

Table 3. Embankment fill and geotextile properties.

		First 0.7 m	Remainder of fill
Material properties of embankment fill	c' (kPa)	0	17.5
	ϕ'	43°	38°
	ψ	8°	7°
	γ (kN/m ³)	18.0	19.6
	ν	0.35	0.35
Janbu's equation	K_E	250	250
	m	0.5	0.5
Geotextile stiffness		ϵ (from 0–1%)	$1 < \epsilon \leq 13$
	J (kN/m)	400	1920

Fig. 6. Comparison of calculated and measured vertical displacements at settlement plates 6S, 7S, and 8S.



Comparison of calculated and measured displacements

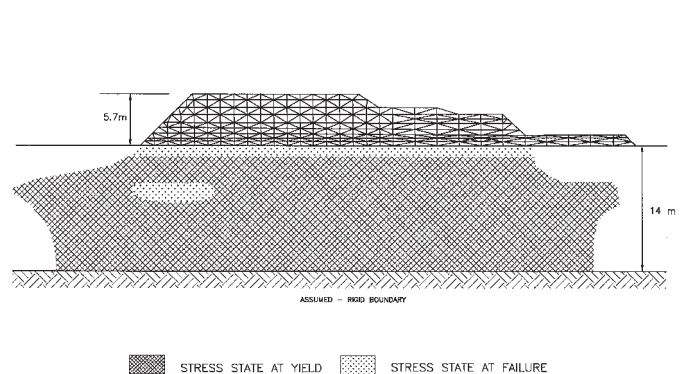
Embankment side slopes

Although it was initially intended that the Sackville test embankment be constructed with nominal 1:1 ($H:V$) side slopes, the survey data indicate that the slope varied between 1:1 and 1.3:1 with an average slope during construction of approximately 1.25:1. To assess the effects of the Embankment side slopes on the calculated behaviour, the Sackville test embankment was analyzed for side slopes of both 1:1 and 1.25:1.

Vertical displacements at 6S, 7S, and 8S

Figure 6 shows the comparison of measured and calculated vertical displacements at settlement plates 6S, 7S, and

Fig. 7. Calculated zones of plasticity at a fill thickness of 5.7 m.



8S for the two side slopes examined. The side slopes had a small effect on the calculated settlements at 7S and 8S. The effect was greatest at 6S and the analyses for slopes of 1:1 and 1.25:1 tend to bracket the observed settlement. In general, the calculated magnitude and trend of vertical displacements at settlement plates 6S, 7S, and 8S are in reasonable agreement with the measured vertical displacements. The discrepancy is greatest as the fill was constructed from 5.7 to 8.2 m thickness as discussed below.

The calculated zones of plasticity shown in Fig. 7 indicate that although a significant portion of the foundation soil has yielded, the zones of plastic failure within the foundation soil are confined at a fill thickness of 5.7 m. The calculated deformations are dominated by yielding within the foundation soil. The calculated velocity field at a fill thickness of 5.7 m (see Fig. 8) indicates that a collapse mechanism is beginning to develop within the foundation soil (the velocity

Fig. 8. Calculated velocity field at an embankment thickness of 5.7 m. Location of settlement augers 9A, 10A, and 11A, and settlement plates 6S, 7S, and 8S are shown.

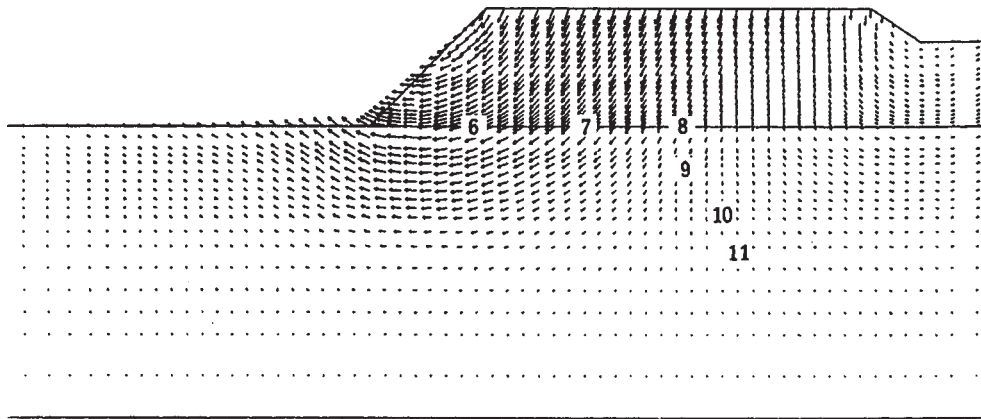
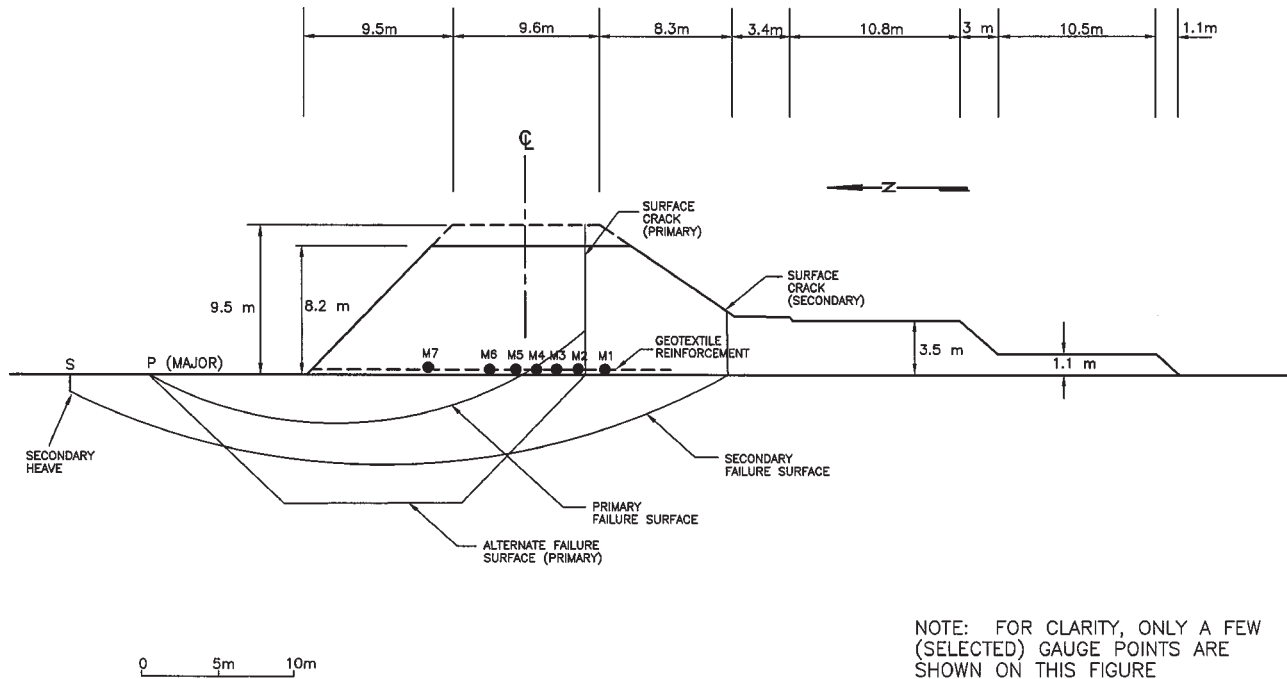


Fig. 9. Inferred failure surfaces and location of mechanical gauge points (from Rowe and Gnanendran 1994).

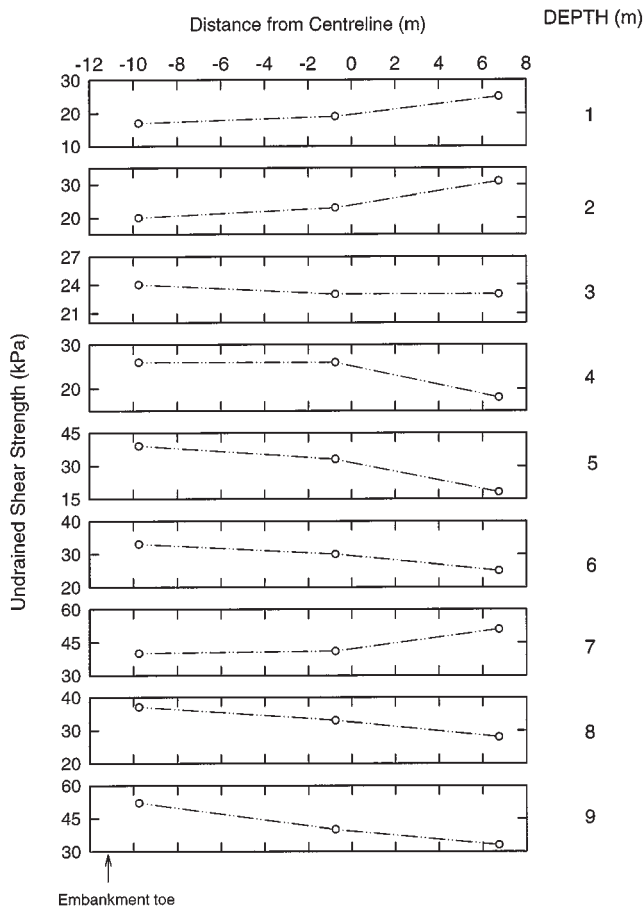


field shows the direction and relative magnitude of an increment in displacement at a series of points over a small increment at this fill level). The position of the potential collapse mechanism shown in Fig. 8 is consistent with the primary failure surface observed during construction of the Sackville test embankment (Fig. 9). Referring to Fig. 8, settlement plates 6S and 7S are within the potential failure mechanism while settlement plate 8S is not. At a fill thickness of 5.7 m, the measured displacements at 6S are in good agreement with the calculated displacements; however, the measured displacements at 7S and 8S exceed calculated displacements. Also, the calculated displacements at 7S exceed the calculated displacement at 8S at a fill thickness of 5.7 m; however, the recorded displacements at 8S exceed the recorded displacements at 7S. The effect of rotations and curvature of the settlement rod for settlement plate 8S was not sufficient to explain this difference. Possible explanations for the

larger vertical displacements at 8S for a fill thickness of 5.7 m may be (i) horizontal nonhomogeneity of foundation shear strength, and (or) (ii) the effects of construction loads.

The variation of field vane shear strengths beneath the Sackville test embankment is shown in Fig. 10. At depths of 1 and 2 m, the vane shear strength beneath the embankment centreline exceeds the vane shear strength beneath the embankment toe. At depths greater than 2.0 m, however, the field vane shear strengths are between 8 and 24% lower beneath the embankment centreline than beneath the embankment toe. The analysis reported herein considered nonhomogeneity in the vertical plane but did not consider nonhomogeneity in the horizontal plane. The reduced shear strength beneath the embankment centreline may result in local yielding, increased plasticity, and hence, increased displacements beneath the embankment centreline. In addition to the reduced foundation shear strength beneath the em-

Fig. 10. Variation of field vane shear strength beneath the Sackville test embankment.



bankment centreline, construction traffic on the access road near the embankment centreline and the filling operations of the bulldozer (which push material up the slope from the access road shown in Fig. 1) may have also increased local yielding and consolidation contributing to the increased measured displacements at settlement plate 8S.

At a full thickness of 8.2 m, the calculated zones of plasticity (Fig. 11) indicate that the failure zone is contiguous within the foundation soil and implies the development of a collapse mechanism shown in Fig. 12. A comparison of the velocity fields at fill thicknesses of 5.7 m (Fig. 8) and 8.2 m (Fig. 12) reveals that the advancement of fill from 5.7 to 8.2 m increases the size of the failure mechanism to include settlement plate 8S. The calculated displacements at 8S begin to exceed the calculated displacements at 7S at a fill thickness of 8.2 m and compare favourably with the measured field displacements. The inclusion of 8S in the collapse mechanism results in a calculated surface displacement profile that is more consistent with the measured surface displacement profile. As previously stated, the calculated displacements at a fill thickness of 5.7 m are dominated by yielding within the foundation soil while at a fill thickness of 8.2 m the calculated settlements are dominated by the development of a collapse mechanism. The agreement between calculated and measured displacements at a fill thickness of 8.2 m suggests that the assumed shear strength profile used to obtain the calculated embankment behaviour is represen-

tative of the average in situ shear strength mobilized along the failure surface.

Vertical displacements at Augers 9A, 10A, and 11A.

Figure 13 shows the comparison of calculated vertical displacements at augers 9A, 10A, and 11A with field measurements that were corrected for the effects of curvature of the auger rods using the horizontal displacement profile measured at inclinometer 25I (see Fig. 1). This correction was significant at fill thicknesses of 5.7 m and greater. Analyses were performed for embankment side slopes of 1:1 and 1.25:1, however, side slope geometry was found to have an essentially negligible effect on the calculated vertical displacements at 9A, 10A, and 11A. The calculated and measured vertical deformations are close for augers 9A and 11A at a fill thickness of 8.2 m. At a fill thickness of 5.7 m, the field measurements exceed the calculated displacements at all auger locations. Again, this may be due to increased plasticity beneath centreline owing to the reduced foundation shear strength (see Fig. 10) and (or) local yielding and plasticity resulting from construction loads. At a fill thickness of 8.2 m, the measured vertical displacements at 10A exceed the calculated vertical displacements. The calculated vertical displacements indicate that the compressive strains in the foundation soil resulting from embankment loads are relatively uniform. This is indicated by the approximately equal difference between calculated displacements between augers 9A and 10A, and 10A and 11A. The field measurements of vertical displacements show that the vertical compressive strains beneath the embankment increase with depth and that increasing the fill thickness from 5.7 to 8.2 m does not increase the compressive strains in the soil layer between 9A and 10A. This may indicate (i) the presence of a soft zone of soil beneath the embankment centreline that was not picked up by the soils investigation and (or) (ii) axial loading of auger 10A. Settlement auger 10A was located at a depth of 4.0 m. At this depth the shear strength of the foundation soil is at a minimum (see Fig. 4) and axial loading of the auger rod may have pushed the auger deeper into the foundation soil. In general, the calculated vertical deformations agree reasonably well with the corrected field measurements.

Net embankment height versus fill thickness

Figure 14 shows the comparison of the calculated and measured net embankment height versus fill thickness response based on displacement measurements at settlement plates 7S, and 8S. Firstly, Fig. 14 shows that the method of analysis adopted in this paper adequately describes the time-dependent nature of the net embankment height versus fill thickness behaviour during construction of the Sackville test embankment. The calculated behaviour is very close to the measured behaviour at all locations. Secondly, Fig. 14 provides support for the application of elasto-viscoplastic theory to model the constitutive response of the foundation soil. During construction periods, the net embankment height versus fill thickness response is essentially linear. During periods of constant embankment loads, the foundation soil deforms in a time-dependent manner that cannot be explained in terms of consolidation alone and the net embankment response becomes more nonlinear with time. In general, the method of analysis closely describes the effects

Fig. 11. Calculated zones of plasticity at a fill thickness of 8.2 m.

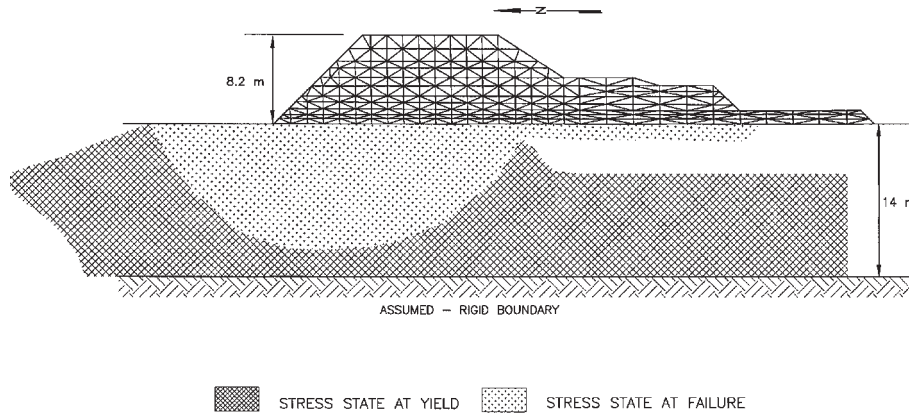
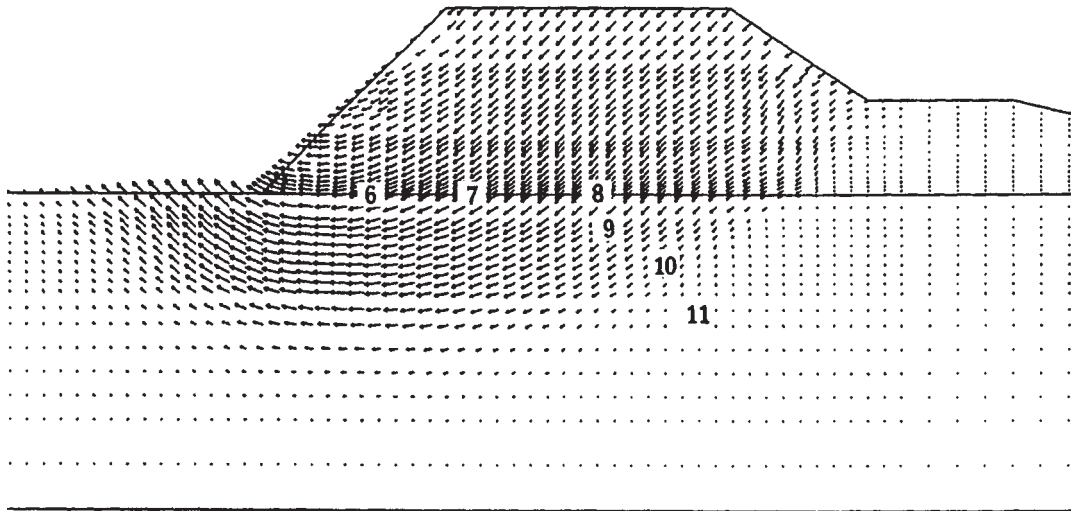


Fig. 12. Calculated velocity field at a fill thickness of 8.2 m. Location of settlement augers 9A, 10A, and 11A, and settlement plates 6S, 7S, and 8S are shown.



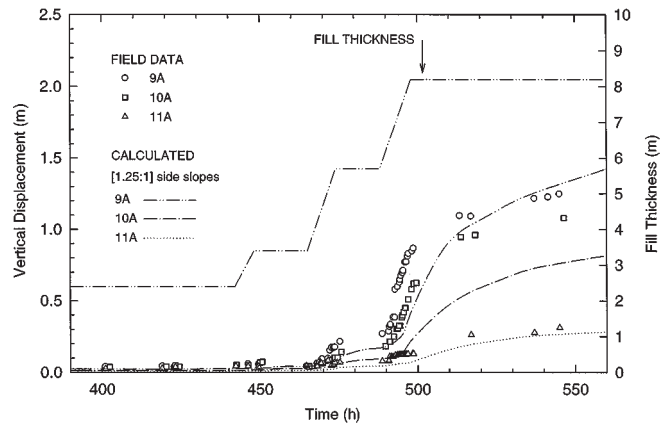
of construction rate and time dependency on the net embankment height behaviour while also considering the effects of pore pressure dissipation.

Vertical displacements at heave plates

The comparison of measured and calculated heave displacements at plates 1H, 2H, and 4H is shown in Fig. 15. Up to a fill thickness of 5.7 m, there is good agreement between the calculated and measured heave at plate 4H for both embankment side slopes of 1:1 and 1.25:1.

At a fill thickness of 8.2 m, the field measurements of heave are relatively uniform ranging from 1.0 m at plate 1H to 1.3 m at plate 2H with an average heave (at the four plates 1H, 2H, 3H, and 4H) of 1.1 m. The calculated heaves for an embankment side slope of 1:1 are nonuniform ranging from 1.6 m at plate 1H to 2.6 m at plate 2H with an average heave of approximately 2 m. For embankment side slopes of 1.25:1, the average calculated heave at a fill thickness of 8.2 m was 1.6 m. This is approaching the measured average heave at the embankment toe; however, the calculated behaviour indicates that embankment side slopes alone cannot account for the relatively uniform measured displacement profile.

Fig. 13. Comparison of calculated vertical displacements with corrected measured displacements at settlement augers 9A, 10A, and 11A — 1.25:1 embankment side slopes.



Some explanation is required for the fact that the agreement between calculated and measured heave near the embankment toe is good for fill thicknesses up to 5.7 m while at a fill thickness of 8.2 m, the measured heave displacement profile becomes more uniform than the calculated profile

Fig. 14. Comparison of calculated and measured net embankment height versus fill thickness.

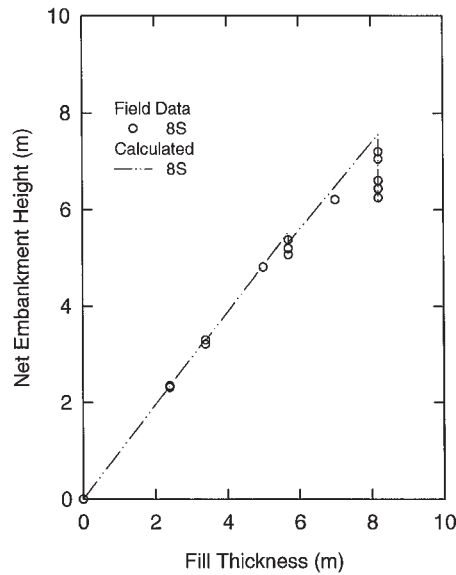
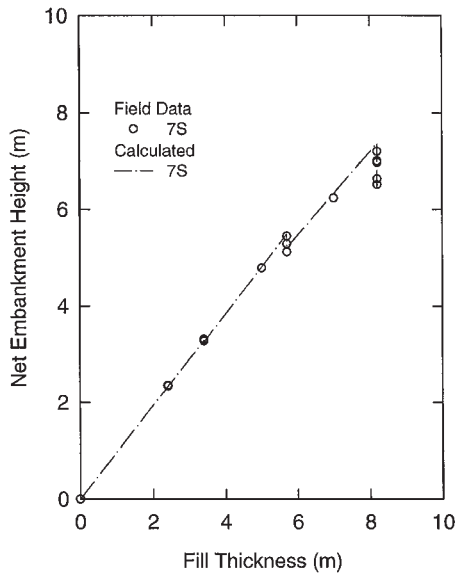
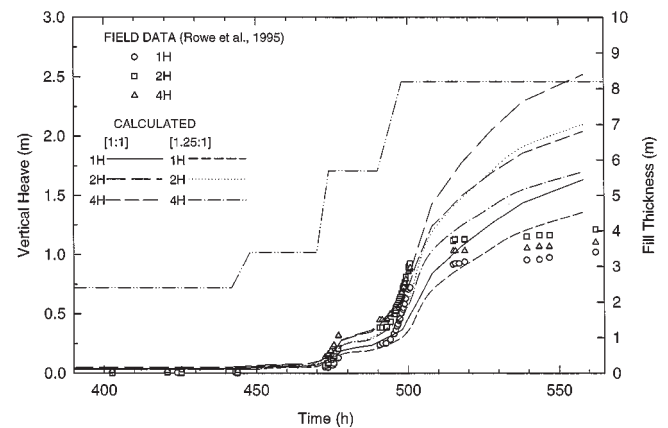


Fig. 15. Comparison of calculated and measured heave at heave plates 1, 2, and 4.

and the calculated heave at heave plates 1H, 2H, and 4H begins to diverge from the measured heave. This may be due to the presence of vertical cuts that were made in the upper 1.0 m of the foundation soil (root mat) to reduce the tensile strength of the surface soils prior to construction of the Sackville test embankment. These cuts did not appear to play a role up to 5.7 m, however Rowe et al. (1995) observed significant “thrust faulting” (predominantly along cuts in the root mat) in the heave zone at a fill thickness of 8.2 m. The thrust faulting appeared to be due to the vertical cuts made in the surface root mat. The present method of analysis does not account for this type of discontinuous deformation at the embankment toe, and hence did model the effect of the discontinuous movement at these joints that appears to have resulted in a more uniform displacement profile than would have been expected without the cuts.

Horizontal displacements

During construction of the Sackville test embankment, horizontal displacements at the embankment toe were monitored using inclinometer 22I and a survey stake for control. Figure 16 shows the comparison of calculated horizontal displacements at the embankment toe (1:1 and 1.25:1 side slopes) with measured displacements for the survey stake at ground level. The calculated and measured horizontal deformations are in good agreement for all fill thicknesses up to and including 8.2 m for the actual 1.25:1 side slopes. The calculated horizontal displacement for the nominal 1:1 embankment side slopes is greater than the measured horizontal displacement for times greater than 498 h. This highlights the significant effect that side slopes can have at fill thicknesses approaching failure. The increasing difference between calculated and measured horizontal displacements at the embankment toe for times greater than 596 h may be due to the combined effects of the thrust faulting, geometric nonlinearity (i.e., rotation and flattening of the embankment side slopes), and three-dimensional effects. The sensitivity to small changes in the embankment side slopes is illustrated



in the figure and the thrust faulting and three dimensional effects cannot be ignored.

The comparison of the measured and calculated profile of horizontal deformations generally showed good agreement at all inclinometers (22I, 23I, 29I, and 25I; see Rowe and Hinchberger 1995). For example, Fig. 17 shows the comparison of calculated relative horizontal displacements with the measured horizontal displacements at inclinometer 23I for fill thicknesses of 3.4 and 5.0 m. The general magnitude and profile of lateral displacements beneath the Sackville test embankment are determined with considerable accuracy using the elasto-viscoplastic elliptical cap constitutive model. As reported by Rowe et al. (1996), poor agreement was obtained using a conventional elastoplastic (Cam-clay) model.

Excess-pore pressure during embankment construction

Figure 18 shows that there is good agreement between the observed and calculated excess pore pressures at the embankment toe and outside the toe (piezometers P24, P25,

Fig. 16. Comparison of calculated and measured horizontal displacements at the embankment toe.

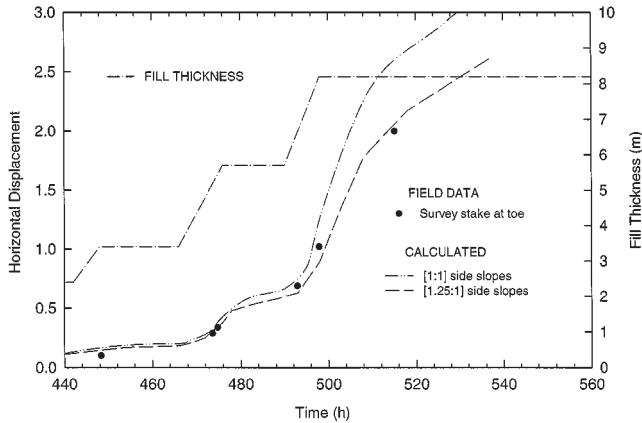


Fig. 17. Calculated and measured relative horizontal displacement profile at inclinometer 231.

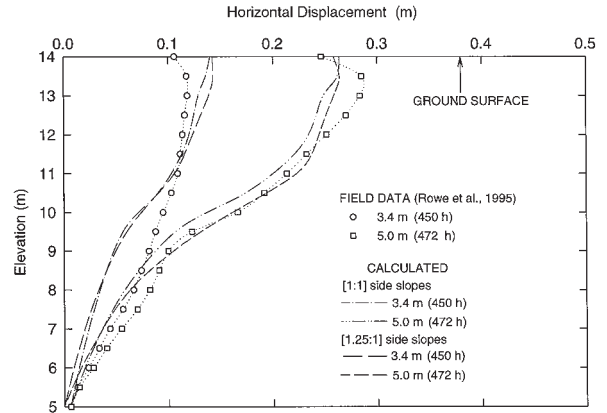


Fig. 18. Comparison of calculated and measured excess pore pressure heads at piezometers 24, 25, 26, and 27.

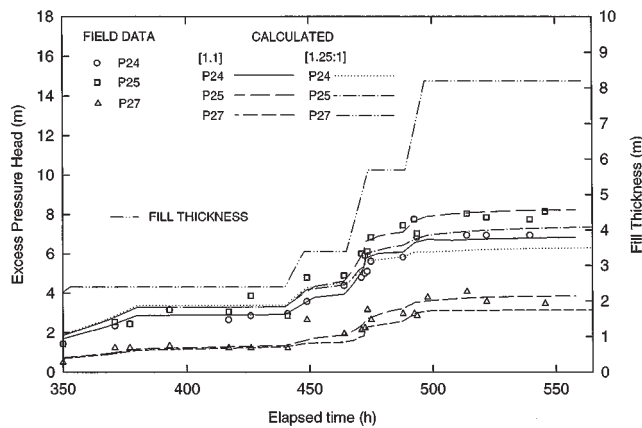


Fig. 19. Comparison of calculated and measured excess pore pressure heads at piezometers 22 and 23.

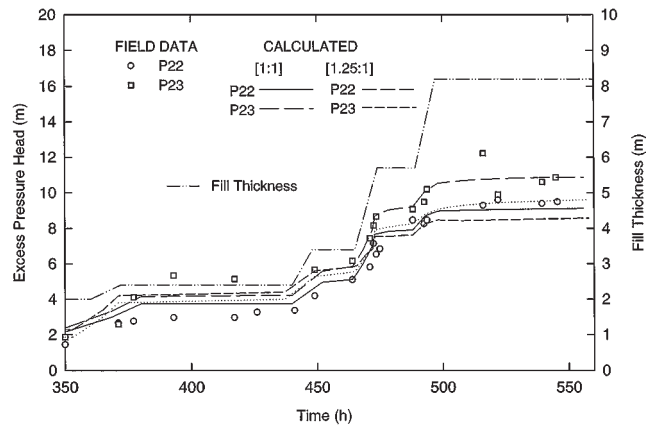
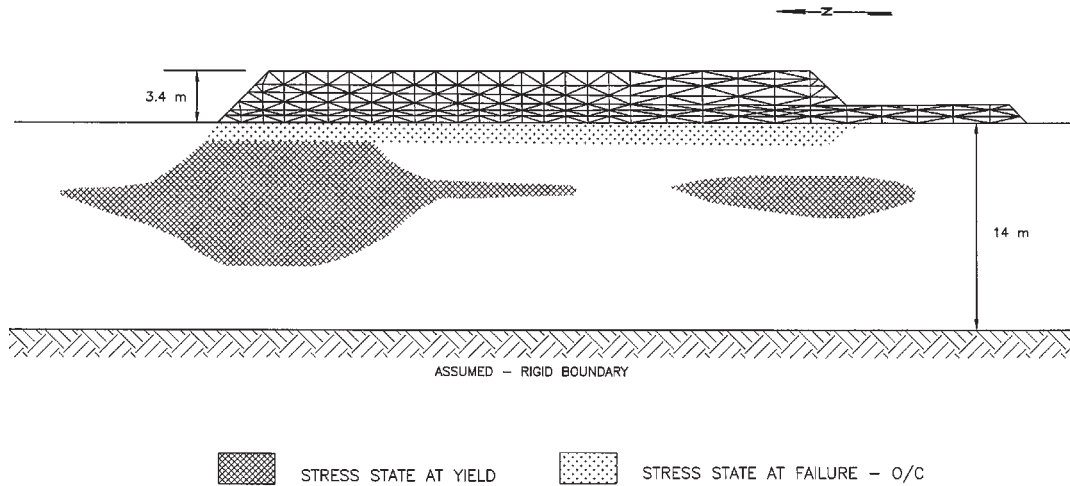


Fig. 20. Calculated zones of yielded soil at a fill thickness of 3.4 m.

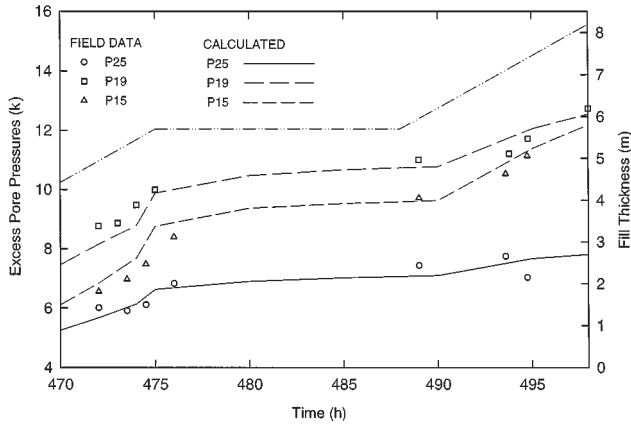


and P27). The calculated excess pore pressures for 1.25:1 embankment side slopes were only slightly less than the calculated excess pore pressures for 1:1 embankment side slopes indicating that the pore pressure at these locations is relatively insensitive to the side slope over this range of val-

ues. (Piezometer P26 is considered to have malfunctioned and is omitted.)

Figure 19 shows good agreement between calculated and measured excess pore pressures at piezometers P22 and P23 located at the midpoint between the embankment toe and

Fig. 21. Excess pore pressures at piezometers 15, 19, and 25 during constant embankment loads (5.7 m fill thickness and 1:1 side slopes).



embankment crest. Similar good agreement was obtained at piezometers P18,30, P19,31, P20, and P21 beneath the embankment crest and P15 and P17 beneath the embankment centreline. The evidence suggests that P16 had a leaking seal.

The excess pore pressures beneath the embankment were observed and predicted to increase with time during periods of constant fill thickness. Since pneumatic piezometers were used to measure the in situ pore pressures, it is unlikely that the increase in excess pore pressures with time is the result of piezometer lag. Referring to Figs. 18 and 19, the pore pressures during construction stoppages remain essentially constant for fill thicknesses below 3.4 m. The time dependency becomes apparent at a fill thickness of 3.4 m and predominant at a fill thickness of 5.7 m. The increased rate dependency of the measured excess pore pressures for fill thicknesses of 3.4 m and greater coincided with the development of significant calculated zones of yielding within the foundation soil that occurred at a fill thickness of 3.4 m (see Fig. 20).

Figure 21 shows a detailed comparison of calculated and measured excess pore pressures at piezometers P15, P19, and P25 during advancement of fill from 3.4 to 5.7 m. During the stoppage of construction at a fill thickness of 5.7 m, the measured excess pore pressures increased by up to 0.7 m during constant embankment loads. The calculated behaviour at piezometers P15, P19, and P25 agrees well with the measured response at all these different locations beneath the embankment.

Reinforcement strains

Reinforcement strains versus fill thickness

Reinforcement strains were measured during the construction of the Sackville test embankment using a variety of electrical and mechanical strain gauges. The measurement of reinforcement strains has been described in detail by Rowe and Gnanendran (1994) and will not be repeated here. Figure 22 shows the comparison of calculated (1.25:1 embankment side slopes) and measured reinforcement strains at a distance of 8.8 m from the embankment toe. The calculated reinforcement strains are close to the measured reinforce-

Fig. 22. Calculated and measured reinforcement strains versus fill thickness (8.8 m from embankment toe).

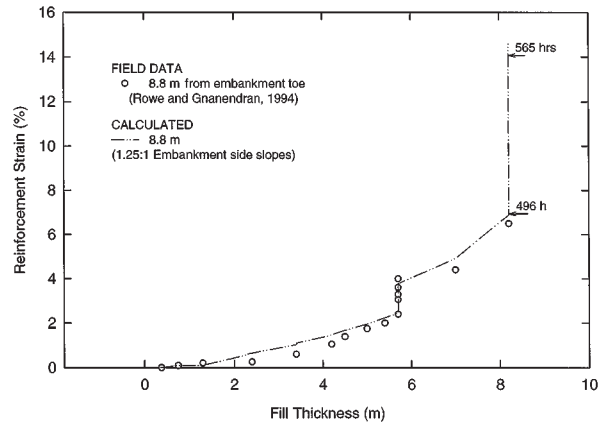
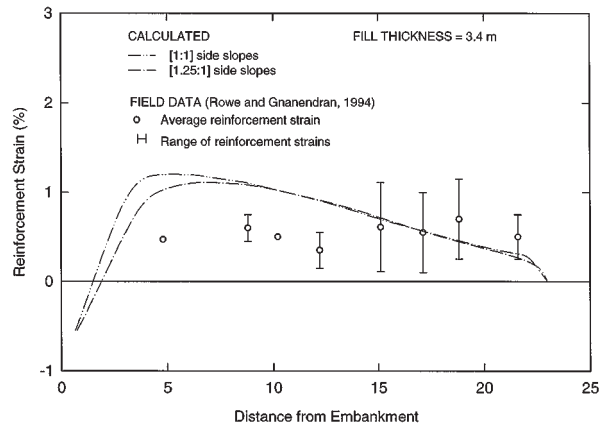


Fig. 23. Calculated and measured reinforcement strain profile at a fill thickness of 3.4 m (450 h).



ment strains for all fill thicknesses. At a fill thickness of 5.7 m, the time-dependent increase of reinforcement strains is closely approximated. Both calculated and measured reinforcement strains increase by approximately 1.8%. The measured reinforcement strains increase to 6.5% at a fill thickness of 8.2 m while the calculated reinforcement strains at a fill thickness of 8.2 m are 6.9%. During the construction stoppage at a fill thickness of 8.2 m, the calculated reinforcement strains at a distance of 8.8 m from the embankment toe increase to 14.0%. The failure strain of the reinforcement was approximately 13%. The calculated maximum reinforcement strain equalled 13% at approximately 550 h (this will be discussed later). Electrical strain gauges installed on the geotextile failed prior to reaching a fill thickness of 8.2 m. Only mechanical gauges were available to monitor reinforcement strains. The mechanical gauges verify the development of large reinforcement strains at a fill thickness of 8.2 m. Similarly, generally good agreement between the development in the geotextile strain with time was obtained at other locations.

Reinforcement strain profiles

Figures 23–25 show the profile of calculated and measured reinforcement strains at fill thicknesses of 3.4 m (450 h), 5.7 m (472 h), and 8.2 m (498 h), respectively. In

Fig. 24. Calculated and measured reinforcement strain profile at a fill thickness of 5.7 m (472 h).

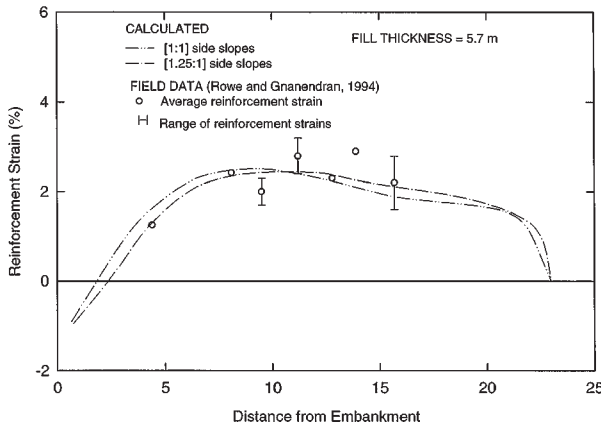
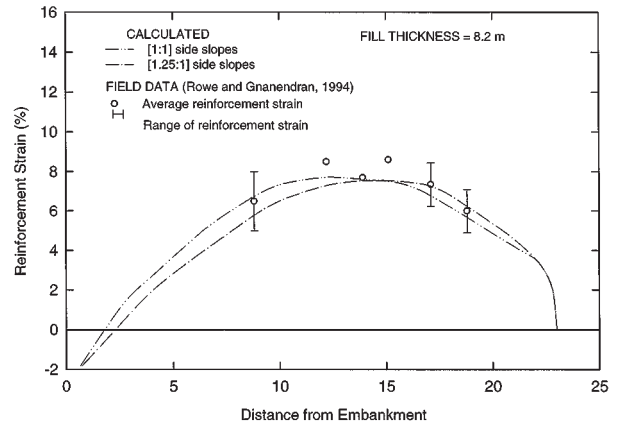


Fig. 25. Calculated and measured reinforcement strain profile at a fill thickness of 8.2 m (498 h).



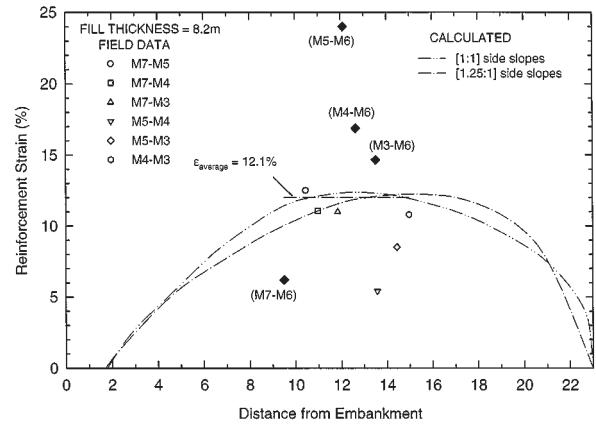
general, the calculated profile of reinforcement strain is close to the measured profile of reinforcement strain at 5.7 m (Fig. 24), 7.0 m (not shown), and 8.2 m (Fig. 25). There is poorer agreement between the calculated and measured profile of reinforcement strain at a fill thickness of 3.4 m. The location of the calculated maximum reinforcement strain is only slightly affected by the side slope geometry and the magnitude of the calculated reinforcement strains are similar for side slopes of 1:1 and 1.25:1, respectively. At 3.4 m thickness (Fig. 23), the calculated strain profile near the embankment toe is close to the measure strain profile with the measured reinforcement strains lower than the calculated values. At distances greater than 12.5 m from the embankment toe, the calculated strain profile continues to decrease while the measured reinforcement strains increase. The increase in measured reinforcement strains may be due to construction loads and increased plasticity beneath centreline resulting from the lower shear strength characteristics of the foundation soil previously discussed.

As the fill thickness is increased, a collapse mechanism develops in the foundation soil and the reinforcement strain profile is dominated by the kinematics of this collapse mechanism. The maximum reinforcement strain and the location of the maximum reinforcement strain based on the average soil strength properties is close to the field measurements of the reinforcement strains for the Sackville test embankment.

Failure of the reinforcement

Figure 9 shows the position of mechanical strain gauges and the inferred position of the failure surface in the field for the Sackville test embankment. Rowe and Gnanendran (1994) reported that, at 498 h, the maximum reinforcement strain between M5 and M6 was approximately 13.9%. By 512 h, the maximum recorded reinforcement strain had increased to about 23% and this was accompanied by a reduction in strain between M4–M5 and M6–M7. This behaviour is consistent with a tear in the geotextile occurring at or near gauge point M5 as hypothesized by Rowe and Gnanendran (1994). At a fill thickness of 8.2 m, the calculated reinforcement strains increased from 6.9% at 496 h to approximately 14% at 565 h. Thus, the analysis also implies failure of the

Fig. 26. Measured reinforcement strains based on mechanical gauge points at 534 h — Sackville test embankment.



reinforcement at a fill thickness of 8.2 m but at approximately 550 h rather than at about 498 h.

Figure 26 shows the plot of measured reinforcement strains and calculated reinforcement strain profile (1:1 and 1.25:1 side slopes) at 534 h. At a fill thickness of 8.2 m, the calculated profile of reinforcement strain is relatively uniform between gauges M3 and M7; however, between M5 and M6 the measured reinforcement strain is 24% at 534 h. This suggests failure of the reinforcement; however, if the failure extended any significant distance from the monitoring points then one would expect that the tear of the reinforcement between M5 and M6 would be accompanied by a significant increase in both the relative displacements between 7S–8S, M5–M7, M4–M7, and M3–M7 and the displacements within the primary failure mass at S6, S7, and S8. Since large changes were not observed, some explanation is required. One possible explanation for this behaviour is that three-dimensional effects resulted in a local tear between M5–M6 that did not propagate through the entire width of the reinforcement. While it is not possible to confirm this hypothesis, it is consistent with both the field observations and the findings of the theoretical analysis. The calculated behaviour presented in this paper supports the hypothesis that, at 534 h, the average reinforcement strain between M3 and M7 is approximately 12% and that, although there was local failure of the reinforcement as implied by

the strain measurements, much of the reinforcement remained intact during constant embankment loads at a fill thickness of 8.2 m up to approximately 550 h. It is considered that the absence of a dramatic change in behaviour (e.g., sudden collapse) or accelerated rates of displacement is due to (a) the ability of this visco-plastic soil at Sackville to support short term overstress (and hence absorb much of the energy that would be released by failure of the reinforcement) and (b) either a three-dimensional redistribution of stress when the reinforcement progressively failed or pullout of the reinforcement.

Summary and discussion

The ability of the elasto-viscoplastic elliptical cap model to describe the measured vertical and horizontal displacements during construction of the Sackville test embankment has been demonstrated. The magnitude and the general time dependency of the vertical deformations at settlement plates 6S, 7S, and 8S and settlement augers 9A, 10A, and 11A are quite reasonably approximated by the method of analysis and the increased deformations recorded during construction stoppages were well described by time-dependent plasticity. Furthermore, the calculated rates of shearing within the foundation soil at a fill thickness of 8.2 m are close to the in situ rates of shearing. The differences between calculated and measured displacements are generally relatively small and are considered to reflect a combination of the effects of the variation of soil properties, three-dimensional effects and the effects of construction loads.

The ability of the method of analysis to simultaneously describe both the vertical and horizontal deformations with considerable success represents a significant improvement over conventional inviscous elastoplastic analyses, which have had little success predicting lateral deformations beneath embankments constructed on soft cohesive foundation soils and often significantly overestimate the lateral deformations (e.g., Rowe et al. 1996). The difficulties associated with the prediction of lateral deformations beneath embankments have been attributed to a number of factors including those discussed by Poulos (1972),

- (i) difficulty estimating Poisson's ratio of the foundation soil
- (ii) anisotropy of the foundation soil;
- (iii) nonlinear stress-strain behaviour of the foundation soil;
- (iv) nonhomogeneity of the foundation soil; and
- (v) incorrect assumptions made regarding the stresses applied to the foundation soil.

Tavenas et al. (1979) studied the lateral deformations developed in soft clay foundations during construction of 21 different embankments and concluded that overprediction of lateral deformations resulted from neglecting the consolidation that occurred during the initial periods of embankment construction.

Anisotropy of the Sackville foundation soil was shown by Gnanendran (1993) to be small and insignificant. Rowe et al. (1996) used a nonlinear elastoplastic Modified Cam-clay constitutive model coupled with Biot consolidation theory to analyze the Sackville test embankment. This analysis considered

- (i) soil nonlinearity,

- (ii) consolidation effects,
- (iii) embankment fill stiffness and
- (iv) soil structure interaction between the embankment fill and reinforcement.

However, the method of analysis also overpredicted the horizontal deformations beneath the Sackville test embankment. Rowe et al. (1996) attributed the problems with predicting the behaviour of the Sackville embankment primarily to limitations of the elastoplastic Cam-clay constitutive relationship that was used. Nonhomogeneity of the Sackville foundation soil may have also been a factor.

The finite element analysis adopted in this paper models the stiffness of the embankment fill materials and considers the transfer of shear and normal stresses resulting from embankment loads to the foundation soil. Furthermore, the consolidation during construction of the test embankment was also considered. A comparison of calculated and measured horizontal deformations showed good agreement, however, the field measurements fluctuated about the calculated profile of horizontal displacements and this is attributed to soil nonhomogeneity. Although the method of analysis considered nonhomogeneity in the vertical plane, it did not consider the nonhomogeneity of the Sackville foundation soil in the horizontal plane. The comparison of calculated and measured horizontal displacements suggests that if engineers can make good practical judgements regarding the average or representative foundation soil properties along the potential failure plane, then nonhomogeneity will only cause in situ displacements to deviate locally from calculated displacements. The analysis reported herein appears to confirm the hypothesis of Rowe et al. (1996) that the difficulties they encountered with predicting the lateral displacements beneath the Sackville test embankment resulted mainly from neglecting the time-dependent characteristics of the Sackville foundation soil at yield and at failure (i.e., the viscoplastic response).

In addition to the displacements recorded during construction of the Sackville test embankment, the method of analysis adopted was also able to closely describe the measured excess pore pressures within the Sackville foundation. For fill thicknesses, which result in yielding within the foundation soil, it was shown that the measured increase in excess pore pressures during periods of constant embankment loads can be described using the elasto-viscoplastic elliptical cap model. Furthermore, significant yielding of the foundation soil was shown to occur at a fill thickness of 3.4 m. The time dependency of the measured in situ excess pore pressures also coincided with a fill thickness of 3.4 m.

The ability of the elasto-viscoplastic analysis to describe the time-dependent development of reinforcement strains during construction of the Sackville test embankment was also illustrated.

Conclusions

A number of conclusions can be drawn from the current study. Firstly, many of the rate sensitive characteristics of the foundation soil and the time-dependent field behaviour of the Sackville test embankment were adequately described using yield surface concepts and time-dependent plasticity.

Secondly, both the observed and calculated excess pore pressures increased during periods when there was no construction and this can be attributed to “creep-induced” pore pressures. This implies that the most critical time with respect to stability may not be during construction but at some time after construction has been completed. This type of failure is often referred to as “progressive failure.”

Thirdly, there is considerable evidence, from both field measurements and calculated behaviour, that the reinforcement yielded/failed during the construction stoppage at 8.2 m. However, there was no sudden or brittle failure but, rather, a quite ductile failure was observed even when the reinforcement appears to have failed. This is contrary to what would be expected for a soil that does not exhibit time-dependent behaviour and is attributed, in part, to the ability of the soil to carry overstress but then creep to failure.

Fourthly, both the field case and the analysis indicate that particular care is required when constructing embankments over rate-sensitive soil such as the Sackville soil. The soils may give the appearance of performing adequately during construction due to the ability of the soil to carry overstress, and they may subsequently creep to failure (as appears to have been the case for the Sackville embankment). A similar example of “progressive failure” has been reported for New Brunswick soil by Keenan et al. (1986).

Finally, to adequately describe all aspects of the field performance of the Sackville test embankment, it was necessary to model the time-dependent characteristics of the Sackville foundation soil at yield and at failure. In view of the success reported in this paper, the elasto-viscoplastic elliptical cap constitutive model appears to be suitable for studying current design methods for reinforced embankments constructed on soft rate sensitive foundation soils similar to the Sackville foundation soil.

Acknowledgement

The analyses reported in this paper were funded by the Natural Sciences and Engineering Research Council of Canada under grant A1007 to Dr. R.K. Rowe.

References

- Adachi, T., and Okano, M. 1974. A constitutive equation for normally consolidated clay. *Soils and Foundations*, **14**: 55–73.
- Carter, J.P., and Balaam, N.P. 1990. AFENA - A general finite element algorithm: users manual. School of Civil Engineering and Mining Engineering, University of Sydney, N.S.W. 2006, Australia.
- Carter, P., Booker, J.R., and Small, J.C. 1979. The analysis of finite elasto-plastic consolidation. *International Journal for Numerical and Analytical Methods in Geomechanics*, **3**: 107–129.
- Chen, W.F. 1982. *Plasticity in reinforced concrete*. McGraw-Hill, New York.
- Davis, E.H. 1968. Theories of plasticity and failure of soil masses. *In Soil mechanics - selected topics*. Edited by I.K. Lee. Butterworths, London. Chap. 6.
- Gnanendran, C.T. 1993. Observed and calculated behaviour of a geotextile reinforced embankment on a soft compressible soil. Ph.D. thesis, University of Western Ontario, London, Ont.
- Hinchberger, S.D. 1996. The behaviour of reinforced and unreinforced embankments on rate sensitive clayey foundations. Ph.D. thesis, University of Western Ontario, London, Ont.
- Janbu, N. 1963. Soil compressibility as determined by oedometer and triaxial tests. *Proceedings of the European Conference on Soil Mechanics and Foundation Engineering*, Wiesbaden, Germany. **1**: 19–25.
- Katona, M.G., and Mulert, M.A. 1984. A viscoplastic cap model for soils and rock. *In Mechanics of Engineering Material*. Edited by C.S. Desai and R.H. Gallagher. J. Wiley, London. Chap. 17.
- Keenan, G.H., Landva, A.O., Valsangkar, A.J., and Comier, R.S. 1986. Performance and failure of test embankment on organic silty clay. *Proceedings of the Conference on Building on Marginal and Derelict Land*, Glasgow. The Institution of Civil Engineers. **2**: 417–428.
- Leroueil, S., Sampson, L., and Bozozuk, M. 1983. Laboratory and field determination of preconsolidation pressures at Gloucester. *Canadian Geotechnical Journal*, **20**: 477–490.
- Morin, P., Leroueil, S., and Samson, L. 1983. Preconsolidation pressure of Champlain clays. Part I. In-situ determination. *Canadian Geotechnical Journal*, **20**: 782–802.
- Perzyna, P. 1963. The constitutive equations for work-hardening and rate sensitive plastic materials. *Proceedings of Vibration Problems*, Warsaw, **4**(3): 281–290.
- Poulos, H.G. 1972. Difficulties in prediction of horizontal deformations of foundations. *ASCE Journal of the Soil Mechanics and Foundations Division*, **98**: 843–848.
- Roscoe, K.H., and Schofield, A.N. 1963. Mechanical behaviour of an idealised “wet clay.” *Proceedings of the Second European Conference on Soil Mechanics*. pp. 47–54.
- Rowe, R.K., and Gnanendran, C.T. 1994. Geotextile strain in a full scale reinforced test embankment. *Geotextiles and Geomembranes*, **13**: 781–806.
- Rowe, R.K., and Hinchberger, S.D. 1995. The significance of rate effects in modelling the Sackville test embankment. *Research Report GEOT-16-95*, Faculty of Engineering Science, University of Western Ontario, London, Ontario. p. 86.
- Rowe, R.K., Gnanendran, C.T., Landva, A.O., and Valsangkar, A.J. 1995. Construction and performance of a full-scale geotextile reinforced test embankment, Sackville, New Brunswick. *Canadian Geotechnical Journal*, **32**: 512–534; *Erratum* **33**: 208, 1996.
- Rowe, R.K., Gnanendran, C.T., Landva, A.O., and Valsangkar, A.J. 1996. Calculated and observed behaviour of a reinforced embankment over soft compressible soil. *Canadian Geotechnical Journal*, **33**: 324–338.
- Tavenas, F., Mieussens, C., and Bourges, F. 1979. Lateral displacements in clay foundations under embankments. *Canadian Geotechnical Journal*, **16**: 532–550.
- Terzaghi, K., and Peck, R.B. 1948. *Soil mechanics in engineering practice*. John Wiley & Sons, New York.

Appendix A

The strain rate of the elasto-viscoplastic material was taken to be the sum of the elastic ($\dot{\epsilon}_{ij}^e$) and visco-plastic ($\dot{\epsilon}_{ij}^{vp}$) strain rates; viz.

$$[A1] \quad \dot{\epsilon}_{ij} = \dot{\epsilon}_{ij}^e + \dot{\epsilon}_{ij}^{vp}$$

For stress states below yield, the elastic bulk modulus, K , was considered to be stress dependent and given by

$$[A2] \quad K = \frac{(1+e)\sigma'_m}{\kappa}$$

where κ is the recompression index, e is the void ratio, and σ'_m is the mean effective stress. The shear modulus, G , is related to the bulk modulus, K , by:

$$[A3] \quad G = \frac{3(1-2\nu)K}{2(1+\nu)}$$

where ν is Poisson's ratio and was assumed to remain constant. The viscoplastic strain rate tensor was given by

$$[A4] \quad \dot{\epsilon}_{ij}^{vp} = \gamma^{vp} \langle \Phi(F) \rangle \frac{\partial f}{\partial \sigma'_{ij}}$$

where γ^{vp} is the viscoplastic fluidity parameter with units of inverse time, the scalar function $\Phi(F)$ is called the flow function, and $\partial f / \partial \sigma'_{ij}$ is the plastic potential for associated viscoplasticity. The elliptical cap yield function (Chen 1982) used to define yielding in the normally consolidated stress range in $\sqrt{2J_2} - \sigma'_m$ stress space has the form:

$$(A5) \quad f^{(s)} = (\sigma'_m - l)^2 + 2J_2 R_c^2 - (\sigma_{my}^{(s)} - l)^2 = 0$$

where l is the σ'_m -coordinate of the centre of the ellipse, $\sigma_{my}^{(s)}$ is the yield surface intercept with the σ'_m -axis, R_c is the yield surface aspect ratio in $\sqrt{2J_2} - \sigma'_m$ space, and is the second invariant of the deviatoric stress tensor.

The elasto-viscoplastic constitutive equation associated with the elliptical cap yield surface in the normally consolidated stress range then becomes:

$$[A6] \quad \dot{\epsilon}_{i,j} = \frac{\dot{s}_{i,j}}{2G} + \frac{\kappa}{3(1+e)} \frac{\dot{\sigma}'_m}{\sigma'_m} \delta_{i,j} + \gamma^{vp} \langle \Phi(F) \rangle \left[\frac{\delta_{i,j}}{3} - \left(\frac{2l}{\sigma_{my}^{(d)}} - 1 \right) \left(\frac{\sigma_{my}^{(d)}}{\sigma'_m} \right)^2 \frac{\delta_{i,j}}{3} - R_c^2 \left(\frac{\sqrt{2J_2}}{\sigma'_m} \right)^2 \frac{\delta_{i,j}}{3} + \frac{2s_{i,j} R_c^2}{\sigma'_m} \right] \Phi(F) = \left(\frac{\sigma_{my}^{(s)} + \sigma_{os}^{(d)}}{\sigma_{my}^{(s)}} \right)^n$$

where s_{ij} is the deviatoric stress tensor, δ_{ij} is Kronecker's delta, n is the strain rate exponent, $\sigma_{my}^{(d)}$ is the dynamic yield surface intercept, $\sigma_{os}^{(d)}$ is the overstress function, and all other parameters are as previously defined. The expansion of the yield surface is a time-dependent process depending on the current viscoplastic increment of volumetric strain, $\partial \epsilon_{vol}^{vp}$, viz.

$$[A7] \quad \partial \sigma_{my}^{(s)} = \frac{(1+e)}{(\lambda - \kappa)} \sigma_{my}^{(s)} \partial \epsilon_{vol}^{vp}$$

(Roscoe and Schofield 1963) where λ is the compression index.

In the over-consolidated stress range, failure was defined using the Drucker-Prager failure envelope:

$$[A8] \quad f_{(s)} = M^* \sigma'_m + c'_k - \sqrt{2J_2} = 0$$

where M^* is the slope of the failure envelope in $\sqrt{2J_2} - \sigma'_m$ stress space, and c'_k is the cohesion intercept of the failure envelope in $\sqrt{2J_2} - \sigma'_m$ stress space. The elasto-viscoplastic constitutive equation in the over-consolidated stress range then becomes

$$[A9] \quad \dot{\epsilon}_{i,j} = \frac{\dot{s}_{i,j}}{2G} + \frac{\kappa}{3(1+e)} \frac{\dot{\sigma}'_m}{\sigma'_m} \delta_{i,j} + \gamma^{vp} \langle \Phi(F) \rangle \left[\frac{s_{i,j}}{\sqrt{2J_2}} - M^* \frac{\delta_{i,j}}{3} \right], \quad \Phi(F) = \left(\frac{\sigma_{my}^{(s)} + \sigma_{os}^{(d)}}{\sigma_{my}^{(s)}} \right)^n$$

List of symbols

C_c : compression index ($\log_{10} \sigma'$)

C_k : slope of e - $\log(k)$ plot

c' : effective cohesion intercept in $(\sigma'_1 - \sigma'_3) / 2 - \sigma'_m$ stress space

c'_k : effective cohesion intercept in $\sqrt{2J_2} - \sigma'_m$ stress space

E' : Young's modulus

e_0 : initial void ratio

e_r : reference void ratio for relationship

G : shear modulus

K : bulk modulus of elasticity

K_F : material constants for Janbu's equation

K_0 : coefficient of lateral earth pressure at rest

k_r : reference permeability (hydraulic conductivity) for e - $\log(k)$ relationship

k_h : horizontal permeability (hydraulic conductivity)

k_v : vertical permeability (hydraulic conductivity)

l : σ'_m : coordinate of the centre of the elliptical yield surface function

J_2 : second invariant of deviatoric stress tensor

M : slope of Drucker-Prager failure envelope in $\sqrt{2J_2} - \sigma'_m$ stress space

M^* : slope of Drucker-Prager failure envelope in overconsolidated stress range

m : exponent in Janbu's equation

n : strain rate exponent

P_a : atmospheric pressure

R_c : elliptical yield surface aspect ratio in $\sqrt{2J_2} - \sigma'_m$ stress space	κ : recompression index
R_k : ratio of horizontal to vertical permeability $=k_h/k_v$	λ : compression index
t : time	$\Phi(F)$: viscoplastic flow function
γ : bulk unit weight	ϕ' : effective friction angle
γ^{VP} : fluidity constant for viscoplastic analysis	ν : Poisson's ratio
γ_{fill} : bulk unit weight of embankment fill	$\sigma'_{i,j}$: effective stress tensor
$\delta_{i,j}$: Kronecker's delta	σ'_m : mean effective stress $=(\sigma'_1 + \sigma'_2 + \sigma'_3) / 3$
$\dot{\epsilon}_{i,j}$: total strain rate tensor	$\sigma_{my}^{(s)}$: static yield surface intercept
$\dot{\epsilon}_{i,j}^e$: elastic strain rate tensor	$\sigma_{my}^{(d)}$: dynamic yield surface intercept
$\dot{\epsilon}_{i,j}^{VP}$: viscoplastic strain rate tensor	$\sigma_{ps}^{(d)}$: overstress function
$\partial \epsilon_{vol}^{VP}$: incremental volumetric viscoplastic strain	σ_1 : major principal effective stress
$\partial f / \partial \sigma'_{i,j}$: plastic potential	σ_2 : intermediate principal effective stress
	σ_3 : minor principal effective stress